Highly Efficient OLEDs with Phosphorescent Materials

Edited by
Hartmut Yersin

WILEY-VCH Verlag GmbH & Co. KGaA

Highly Efficient OLEDs with Phosphorescent Materials

Edited by
Hartmut Yersin

Related Titles

Schwoerer, M., Wolf, H.C.

Organic Molecular Solids

2007
ISBN 978-3-527-40540-4

Heinzel, T.

Mesoscopic Electronics in Solid State Nanostructures

2007
ISBN 978-3-527-40638-8

Müllen, K., Scherf, U. (eds.)

Organic Light Emitting Devices

Synthesis, Properties and Applications

2006
ISBN 978-3-527-31218-4

Brütting, W. (ed.)

Physics of Organic Semiconductors

2005
ISBN 978-3-527-40550-3

Highly Efficient OLEDs with Phosphorescent Materials

Edited by
Hartmut Yersin

WILEY-VCH Verlag GmbH & Co. KGaA

The Editor

Prof. Dr. Hartmut Yersin
University of Regensburg
Institute of Physical Chemistry
Universitätsstr. 31
93040 Regensburg
Germany

Cover
"Highly efficient organic light emitting diodes with doped transport layers and triplet emitters (red and green), courtesy of Fraunhofer-Institut für Photonische Mikrosysteme (IPMS), Dresden, Germany.

Library of Congress Card No.:
applied for

British Library Cataloguing-in-Publication Data
A catalogue record for this book is available from the British Library.

Bibliographic information published by the Deutsche Nationalbibliothek
The Deutsche Nationalbibliothek lists this publication in the Deutsche Nationalbibliografie; detailed bibliographic data are available in the Internet at <http://dnb.d-nb.de>.

Composition SNP Best-set Typesetter Ltd., Hong Kong

Printing Betz-Druck GmbH, Darmstadt

Bookbinding Litges & Dopf GmbH, Heppenheim

Printed in the Federal Republic of Germany
Printed on acid-free paper

ISBN: 978-3-527-40594-7

Contents

Preface *XIII*
Contributors *XV*

1 Triplet Emitters for Organic Light-Emitting Diodes: Basic Properties *1*
Hartmut Yersin and Walter J. Finkenzeller
1.1 Introduction *1*
1.2 Electro-Luminescence and the Population of Excited States *3*
1.2.1 Multilayer Design of an OLED *3*
1.2.2 Electron–Hole Recombination, Relaxation Paths, and Light Emission *7*
1.3 Electronic Excitations and Excited States *11*
1.3.1 Ligand-Centered (LC) Transitions: States and Splittings *11*
1.3.2 Metal-Centered Transitions and States *15*
1.3.3 Metal-to-Ligand Charge Transfer/Ligand-Centered Transitions: States in Organo-Transition Metal Triplet Emitters *18*
1.3.3.1 Introductory MO Model and Energy States *18*
1.3.3.2 Extended MO Model and Energy States *20*
1.3.3.3 Spin–Orbit Coupling, Triplet Substates, Zero-Field Splitting, and Radiative Decay Rates *24*
1.4 Zero-Field Splitting (ZFS) of the Emitting Triplet, Photophysical Trends, and Ordering Scheme for Organo-Transition Metal Compounds *29*
1.4.1 Ordering Scheme *31*
1.4.2 Photophysical Properties and ZFS *34*
1.4.2.1 Singlet–Triplet Splitting *36*
1.4.2.2 Intersystem Crossing Rates *37*
1.4.2.3 Emission Decay Time and Photoluminescence Quantum Yield *38*
1.4.2.4 Zero-Field Splitting – Summarizing Remarks *38*
1.4.2.5 Emission Band Structures and Vibrational Satellites *39*

1.4.2.6 Localization/Delocalization and Geometry Changes in the Excited Triplet State *39*
1.5 Characterization of the Lowest Triplet State Based on High-Resolution Spectroscopy: Application to $Pt(thpy)_2$ *40*
1.5.1 Highly Resolved Electronic Transitions *42*
1.5.2 Symmetry and Grouptheoretical Considerations *43*
1.6 Characterization of the Lowest Triplet State Based on Decay Time Measurements: Application to $Ir(ppy)_3$ *45*
1.7 Phosphorescence Dynamics and Spin–Lattice Relaxation: Background and Case Study Applied to $Pt(thpy)_2$ *49*
1.7.1 Processes of Spin–Lattice Relaxation *49*
1.7.1.1 The Direct Process *49*
1.7.1.2 The Orbach Process *50*
1.7.1.3 The Raman Process *51*
1.7.2 Population and Decay Dynamics of the Triplet Substates of $Pt(thpy)_2$ *51*
1.8 The Triplet State Under Application of High Magnetic Fields: Properties of $Ir(btp)_2(acac)$ *56*
1.9 Vibrational Satellite Structures: Case Studies Applied to $Pt(thpy)_2$ and $Ir(btp)_2(acac)$ *63*
1.9.1 Vibrational Satellites: Background *63*
1.9.1.1 Franck–Condon Activity *64*
1.9.1.2 Herzberg–Teller Activity *67*
1.9.2 $Pt(thpy)_2$ Emission: Temperature- and Time-Dependence of the Vibrational Satellite Structure *68*
1.9.2.1 Herzberg–Teller-Induced Emission from Substate I: The 1.3 K Spectrum *69*
1.9.2.2 Franck–Condon Activity in the Emissions from Substates II and III: The 20 K Spectrum *70*
1.9.2.3 Time-Resolved Emission and Franck–Condon/Herzberg–Teller Activities *72*
1.9.3 $Ir(btp)_2(acac)$ Emission: Low-Temperature Vibrational Satellite Structure *75*
1.10 Environmental Effects on Triplet State Properties: Case Studies Applied to $Ir(btp)_2(acac)$ *76*
1.10.1 Energy Distribution of Sites *77*
1.10.2 Zero-Field Splittings at Different Sites *78*
1.10.3 Emission Decay and Spin–Lattice Relaxation Times *80*
1.11 Emission Linewidths and Spectral Broadening Effects *81*
1.11.1 Inhomogeneous Linewidths *81*
1.11.2 Homogeneous Linewidths *82*
1.11.3 Line Broadening Effects on the Example of $Pt(thpy)_2$ *85*
1.11.4 Phenomenological Simulation of Spectral Broadening *86*
1.12 Conclusions *89*

2 Spin Correlations in Organic Light-Emitting Diodes *99*
Manfred J. Walter and John M. Lupton
2.1 Introduction *99*
2.2 Spin-Dependent Recombination of Charge Carriers and Spin-Lattice Relaxation *103*
2.3 Studying Spin States using Electric Field Modulated Fluorescence and Phosphorescence *107*
2.3.1 Electric Field Modulation of Fluorescence and Phosphorescence: Experimental Method *107*
2.3.2 Estimating the Triplet Formation Rate from Transient Electroluminescence *113*
2.3.3 Spin Persistence in Charge Carrier Pairs Generated by an Electric Field *114*
2.3.4 Spin Persistence in Charge Carrier Pairs Generated Spontaneously *119*
2.4 Summary and Outlook *125*

3 Cyclometallated Organoiridium Complexes as Emitters in Electrophosphorescent Devices *131*
Peter I. Djurovich and Mark E. Thompson
3.1 Organic Light-Emitting Devices *131*
3.2 Phosphorescent Materials as Emitters in OLEDs *132*
3.3 Organometallic Complexes as Phosphorescent Emitters in OLEDs *134*
3.4 Confining Triplet Excitons and Carriers in Phosphor-Doped OLEDs *136*
3.5 Cyclometallated Complexes for OLEDs *139*
3.5.1 Synthesis of Cyclometallated Ir Complexes *139*
3.5.2 Excited States in Cyclometallated Complexes *140*
3.5.3 MO Analysis of Ir Cyclometallates *142*
3.5.4 Using Ancillary Ligands to Modify the Excited State Properties *143*
3.5.5 Facial and Meridional Isomers of Tris-Cyclometallates *145*
3.5.6 Ancillary Ligands with Low Triplet Energies *146*
3.5.7 Ligand Tuning to Achieve Green to Near-Infrared Emission *148*
3.5.8 Near-UV Luminescent Cyclometallated Complexes *150*
3.6 Conclusion *154*

4 Highly Efficient Red-Phosphorescent Iridium Complexes *163*
Akira Tsuboyama, Shinjiro Okada, and Kazunori Ueno
4.1 Introduction *164*
4.2 Issues of Red-Emissive Materials *165*
4.3 Red-Phosphorescent Iridium Complexes *165*
4.3.1 Lowest Excited State of Iridium Complexes *165*
4.3.2 Molecular Design and Structure *167*
4.3.3 Phosphorescence Spectra *169*

4.3.4 Phosphorescence Yield *171*
4.3.5 Substituent Effects of $Ir(piq)_3$ (6) *173*
4.4 OLED Device *177*
4.4.1 Thermal Stability *177*
4.4.2 Red OLED using $Ir(4F5mpiq)_3$ (10) *179*
4.5 Summary *179*

5 Pyridyl Azolate Based Luminescent Complexes: Strategic Design, Photophysics, and Applications *185*
Yun Chi and Pi-Tai Chou
5.1 Introduction *185*
5.2 Ligand Synthesis *186*
5.2.1 Ligand Modifications *188*
5.2.2 Fluorescent Behavior and Color Tuning *190*
5.3 Phosphorescent OLED Applications *193*
5.3.1 Osmium-Based Emitters *193*
5.3.1.1 Blue-Emitting Materials *193*
5.3.1.2 Red-Emitting Materials *198*
5.3.2 Ruthenium-Based Emitters *203*
5.3.3 Iridium-Based Emitters *207*
5.3.3.1 Tuning the Color to Red *207*
5.3.3.2 Blue-Emitting Materials *209*
5.3.4 Platinum-Based Emitters *212*
5.4 Concluding Remarks *216*

6 Physical Processes in Polymer-Based Electrophosphorescent Devices *221*
Xiao-Hui Yang, Frank Jaiser, and Dieter Neher
6.1 Introduction *221*
6.2 Phosphorescent Devices Based on PVK *223*
6.2.1 Charge Trapping in Devices with $Ir(ppy)_3$ *224*
6.2.2 Competition Between Free Carrier Recombination and Trapping *227*
6.2.3 Competition between Förster Transfer and Trapping *230*
6.2.3.1 Exciplex Emission *235*
6.2.4 Confinement of Singlet and Triplet Excitons on the PVK:PBD Matrix *239*
6.3 Devices with PtOEP Doped into Conjugated Polymer Matrices *243*
6.3.1 PtOEP in MeLPPP *245*
6.3.1.1 Förster Transfer *245*
6.3.1.2 Dexter Transfer *247*
6.3.1.3 Electrophosphorescence *250*
6.3.2 PtOEP in Polyfluorene *250*
6.4 Conclusion and Outlook *251*

7 Phosphorescent Platinum(II) Materials for OLED Applications *259*
Hai-Feng Xiang, Siu-Wai Lai, P. T. Lai, and Chi-Ming Che
7.1 Introduction *259*
7.1.1 Phosphorescent Materials for OLED Applications *259*
7.1.2 Criteria for Complexes as OLED Emitters *260*
7.2 Device Fabrication and Electroluminescence Measurements *260*
7.3 Platinum(II) α-Diimine Arylacetylide Complexes *262*
7.4 Tridentate Pt(II) Complexes *265*
7.4.1 Cyclometalated 6-Aryl-2,2′-bipyridine Arylacetylide Pt(II) Complexes *265*
7.4.2 Pt(II) Complexes bearing 6-(2-Hydroxyphenyl)-2,2′-bipyridine Ligands *268*
7.5 Tetradentate Pt(II) Complexes *270*
7.5.1 Pt(II) Schiff Base Complexes *270*
7.5.2 Pt(II) Bis(phenoxy)diimine Complexes *273*
7.5.3 Pt(II) Bis(pyrrole)diimine Complexes *276*
7.5.4 Pt(II) Porphyrin Complexes *277*
7.6 Concluding Remarks *279*

8 Energy-Transfer Processes between Phosphorescent Guest and Fluorescent Host Molecules in Phosphorescent OLEDs *283*
Isao Tanaka and Shizuo Tokito
8.1 Introduction *283*
8.2 Electronic Structure and Energy Transfer in Guest–Host Systems *284*
8.3 Luminescence Properties of Phosphorescent and Fluorescent Materials *286*
8.4 Energy Transfer of Blue Phosphorescent Molecules in Guest–Host Systems *288*
8.5 Energy Transfer Between $Ir(ppy)_3$ and Alq_3: Enhancement of Phosphorescence from Alq_3 *294*
8.6 Energy Transfer Between $Ir(ppy)_3$ and BAlq: Observation of Thermal Equilibrium of Triplet Excited States *301*
8.7 Conclusion *306*

9 High-Efficiency Phosphorescent Polymer LEDs *311*
Addy van Dijken, Klemens Brunner, Herbert Börner, and Bea M.W. Langeveld
9.1 Introduction *311*
9.2 The Route Toward High-Efficiency OLEDs *312*
9.3 Singlet and Triplet Excited States *312*
9.4 Phosphorescent Emitters *313*
9.5 Host Materials for Phosphorescent Emitters *314*
9.5.1 General Requirements *314*
9.5.2 Carbazole-Based Host Materials *316*

9.5.3 Tuning the Properties of Carbazole Derivatives *318*
9.5.4 Carbazole-Based Polymers for High-Efficiency Phosphorescent pLEDs *322*
9.6 Outlook *325*

10 Electroluminescence from Metal-Containing Polymers and Metal Complexes with Functional Ligands *329*
Chris Shuk Kwan Mak, and Wai Kin Chan
10.1 Introduction *329*
10.2 Traditional Materials Used in OLEDs *330*
10.2.1 Molecular Materials *330*
10.2.2 Polymeric Materials *330*
10.3 Development of Phosphorescent Materials for OLEDS *332*
10.3.1 Small Molecules – Pure Organic Dyes and Organometallic Complexes *333*
10.3.2 Polymeric Materials *334*
10.4 Ruthenium Containing Polymers *335*
10.4.1 Photophysics of Ruthenium Complexes *335*
10.4.2 Examples of Ruthenium Complex Containing Polymers *337*
10.4.3 Ruthenium Complexes for Light-Emitting Devices *339*
10.4.4 Complexes Based on Multifunctional Ligands *343*
10.4.5 Ruthenium Containing Polymers for Light-Emitting Devices *346*
10.4.5.1 EL Devices Based on Ruthenium Complex Containing Nonconjugated Polymers *346*
10.4.5.2 Multifunctional Ruthenium Complex Containing Conjugated Polymers *347*
10.4.5.3 Conjugated Polymers with Pendant Metal Complexes *356*
10.5 Summary *358*

11 Molecular Engineering of Iridium Complexes and their Application in Organic Light Emitting Devices *363*
Mohammad K. Nazeeruddin, Cedric Klein, Michael Grätzel, Libero Zuppiroli, and Detlef Berner
11.1 Introduction *363*
11.1.1 Ligand Field Splitting *364*
11.1.2 Photophysical Properties *365*
11.2 Phosphorescent Iridium Complexes *366*
11.2.1 Tuning of Phosphorescence Colors in Neutral Iridium Complexes *366*
11.2.2 Tuning of Phosphorescence Colors in Cationic Iridium Complexes *369*
11.2.3 Tuning of Phosphorescence Colors in Anionic Iridium Complexes *372*
11.2.3.1 Phosphorescent Color Shift in Anionic Iridium Complexes by Tuning of HOMO Levels *375*

11.2.4 Controlling Quantum Yields in Iridium Complexes *377*
11.3 Application of Iridium Complexes in Organic Light-Emitting Devices (OLEDs) *378*
11.3.1 Standard OLED Device Architecture *379*
11.3.2 Light-Emitting Electrochemical Cell (LEC) Device Architecture *387*

12 Progress in Electroluminescence Based on Lanthanide Complexes *391*
Zu-Qiang Bian and Chun-Hui Huang
12.1 Introduction *391*
12.2 The Device Construction and Operating Principles *393*
12.3 The Red Electroluminescence Based on Europium Complexes *396*
12.4 The Green Electroluminescence Based on Terbium Complexes *404*
12.5 The Near Infrared Electroluminescence Based on Neodymium, Erbium, or Ytterbium Complexes *411*
12.6 The Ligand Emission Electroluminescence Based on Yttrium, Lanthanum, Gadolinium, or Lutetium Complexes *415*
12.7 Conclusion *417*

Index *421*

Preface

For nearly a hundred years, the properties of organo-transition metal compounds have fascinated chemists and physicists from a scientific point of view. Although the enormous potential of these materials for opto-electronic applications was evident since long, a break-through came only about fifteen years ago after the demonstration that these compounds are well suited as emitters in highly efficient OLEDs (organic light emitting diodes). This is due to the specific properties of these materials with regard to the electroluminescent processes. In OLEDs, light emission proceeds via a recombination of electrons and holes leading to the formation of 25% singlet and 75% triplet excitons. The 75% triplet excitons are transferred into heat and hence are lost for the generation of light, unless spin-orbit coupling (SOC) induced by a transition metal ion opens a radiative path for the emission from the excited triplet to the singlet ground state. SOC induces also an efficient transfer from the populated 25% singlets to the emitting triplets. Thus, the total excitation energy is transferred to the emitting triplet states. This process is called *triplet harvesting*. In particular, due to these effects, OLEDs which contain organo-transition metal triplet emitters (phosphorescent emitters) can reach a four times higher efficiency than OLEDs built with purely organic singlet emitters (fluorescent emitters). Therefore, this book focuses on phosphorescent emitter materials, their photophysical properties, and their applications in OLEDs.

OLEDs have already started to be commercially applied in small and bright displays and entered the market which hitherto is governed by LCD or other technologies. Lighting by OLEDs comes also into the focus of commercial interests, since efficient and thin large-area lighting sources will become available in near future. The development of these new technologies is characterized by an exceptional interdisciplinary research in the fields of physics, chemistry, and material sciences. Thus, basic research meets applied sciences and industrial interests. Vice versa, the interplay in this field strongly stimulates basic sciences and fundamental material research. Hence, it can be expected that a number of fascinating new materials will be developed in the near future.

In this volume, leading scientists present comprehensive reviews, which provide insight into the emission properties of organo-metallic triplet emitters, the mecha-

nisms of electroluminescence, the development of new emitter and host materials, and the improvement of OLED efficiencies by optimizing the emitter materials and the device architectures. The different contributions are written in a style which enables researchers from related fields and industrial laboratories as well as graduate students to follow the highly informative presentations. I am convinced that the contributions demonstrate the attractiveness and the great potential of the compounds and that further studies towards a better understanding of optoelectronic properties and mechanisms are induced. This will not only open large-scale applications of OLED displays and lighting systems, but will also stimulate the research and development of future applications in organic electronics, such as electrically pumped lasers or highly efficient and inexpensive organic solar cells.

Regensburg, Germany
August, 2007

Hartmut Yersin

List of Contributors

Detlef Berner
CFG Microelectronic
Avenue de Lonay 2-2bis
1110 Morges
Switzerland

Zu-Qiang Bian
Beijing National Laboratory for Molecular Sciences
State Key Laboratory of Rare Earth Materials Chemistry and Applications
Peking University
Beijing, 100871
P.R. China

Herbert Börner
Royal Philips Electronics
Philips Research Europe – Aachen
Weisshausstrasse 2
52066 Aachen
Germany

Klemens Brunner
Royal Philips Electronics
Philips Research Europe – Eindhoven
High Tech Campus 4
5654 AE Eindhoven
The Netherlands

Wai Kin Chan
Department of Chemistry
The University of Hong Kong
Pokfulam Road
Hong Kong
P.R. China

Chi-Ming Che
Department of Chemistry and HKU-CAS Joint Laboratory on New Materials
The University of Hong Kong
Pokfulam Road
Hong Kong
P.R. China

Yun Chi
Department of Chemistry
National Tsing Hua University
101, Section 2, Kuang Fu Road
Hsinchu, 30013
Taiwan

Pi-Tai Chou
Department of Chemistry
National Taiwan University
1, Section 4, Roosevelt Road
Taipei, 10617
Taiwan

Addy van Dijken
Royal Philips Electronics
Philips Research Europe—Eindhoven
High Tech Campus 4
5654 AE Eindhoven
The Netherlands

Peter I. Djurovich
Department of Chemistry
University of Southern California
840 W. 36th Place/Downey Way
Laird J. Stabler Labs, Room 368
Los Angeles, CA 90089
USA

Walter J. Finkenzeller
Institut für Physikalische Chemie
Universität Regensburg
Universitätsstr. 31
93040 Regensburg
Germany

Michael Grätzel
Laboratory for Photonics and Interfaces
Institute of Chemical Sciences and Engineering
School of Basic Sciences
Swiss Federal Institute of Technology
1015 Lausanne
Switzerland

Chun-Hui Huang
Beijing National Laboratory for Molecular Sciences
State Key Laboratory of Rare Earth Materials Chemistry and Applications
Peking University
Beijing, 100871
P.R. China

Frank Jaiser
Physik weicher Materie
Universität Potsdam
Am Neuen Palais 10
14469 Potsdam
Germany

Cedric Klein
Laboratory for Photonics and Interfaces
Institute of Chemical Sciences and Engineering
School of Basic Sciences
Swiss Federal Institute of Technology
1015 Lausanne
Switzerland

P. T. Lai
Department of Electrical and Electronic Engineering
The University of Hong Kong
Pokfulam Road
Hong Kong
P.R. China

Siu-Wai Lai
Department of Chemistry and HKU-CAS Joint Laboratory on New Materials
The University of Hong Kong
Pokfulam Road
Hong Kong
P.R. China

Bea M. W. Langeveld
TNO Science and Industry
De Rondom 1
5600 HE Eindhoven
The Netherlands

John M. Lupton
Department of Physics
University of Utah
115 South 1400 East
Salt Lake City
UT 84112-0830
USA

Chris Shuk Kwan Mak
Department of Chemistry
The University of Hong Kong
Pokfulam Road
Hong Kong
P.R. China

Mohammad K. Nazeeruddin
Laboratory for Photonics and Interfaces
Institute of Chemical Sciences and Engineering
School of Basic Sciences
Swiss Federal Institute of Technology
1015 Lausanne
Switzerland

Dieter Neher
Physik weicher Materie
Universität Potsdam
Am Neuen Palais 10
14469 Potsdam
Germany

Shinjiro Okada
Leading-Edge Technology Development Headquarters
Canon Inc.
5-1 Morinosato-Wakamiya
Atsugi-shi
Kanagawa 243-0193
Japan

Isao Tanaka
NHK (Japan Broadcasting Corporation)
Osaka Broadcasting Station
Technical and Engineering Division
Otemae, Chuo-ku
540-8501 Osaka
Japan

Mark E. Thompson
Department of Chemistry
University of Southern California
840 W. 36th Place/Downey Way
Laird J. Stabler Labs, Room 368
Los Angeles, CA 90089
USA

Shizuo Tokito
NHK (Japan Broadcasting Corporation)
Science and Technical Research Laboratories
Materials Science and Advanced Devices
Kinuta, Setagaya-ku
157-8510 Tokyo
Japan

Akira Tsuboyama
Leading-Edge Technology Development Headquarters
Canon Inc.
5-1 Morinosato-Wakamiya
Atsugi-shi
Kanagawa 243-0193
Japan

Kazunori Ueno
Leading-Edge Technology Development Headquarters
Canon Inc.
5-1 Morinosato-Wakamiya
Atsugi-shi
Kanagawa 243-0193
Japan

Manfred J. Walter
Photonics & Optoelectronics Group
Physics Department and CeNS
Ludwig-Maximilians-Universität München
Amalienstr. 54
80799 München
Germany

Hai-Feng Xiang
Department of Chemistry and HKU – CAS Joint Laboratory on New Materials
The University of Hong Kong
Pokfulam Road
Hong Kong
P.R. China

Xiao-Hui Yang
Arizona State University
School of Materials and Flexible Display Center
7700 South River Parkway
Tempe, AZ 85284
USA

Hartmut Yersin
Institute of Physical Chemistry
University of Regensburg
Universitätsstr. 31
93040 Regensburg
Germany

Libero Zuppiroli
Laboratoire d'Optoélectronique desMatériaux Moléculaires
Institut des Matériaux
Ecole Polytechnique Fédérale
1015 Lausanne
Switzerland

1
Triplet Emitters for Organic Light-Emitting Diodes: Basic Properties

Hartmut Yersin and Walter J. Finkenzeller*

1.1
Introduction

Within the past decade, organo-transition metal compounds consisting of triplet emitters have become highly attractive, in particular, due to their applicability in electro-luminescent devices such as organic light-emitting diodes (OLEDs). With this new technology, efficient light-emitting systems are evolving. For example, in the future it will become possible to fabricate large and brilliant flat panel displays at a moderate price, to prepare illuminating wallpapers, and micro displays for all types of application. One important requirement for all of these applications is low power consumption and high efficiency of the light-emitting devices. Here, the organo-transition metal compounds offer a great advantage. The maximum obtainable efficiency may be a factor of *four* higher than for purely organic emitter materials. Thus, many research groups, both from academic and industrial laboratories, have become interested in this challenging scientific- and application-driven field [1–40].

Organo-transition metal compounds, such as the famous $Ir(ppy)_3$ or $[Ru(bpy)_3]^{2+}$ complexes,[1)] represent triplet emitters. This means, they exhibit an emission – a phosphorescence – from the lowest excited electronic triplet state to the electronic singlet ground state. Although this electronic transition is formally forbidden, it may become sufficiently allowed by spin–orbit coupling (SOC) induced by the central metal. Depending on the specific compound, the emission can show widely differing properties. Its wavelength can lie in the spectral range from blue to red, or even from ultraviolet to infrared. Normally, at ambient temperature, the spectra are not resolved line emissions, but rather are broad and often exhibit an undesirably low color purity. The emission decay time ranges from shorter than 1 µs to as long as several milliseconds, and the photoluminescence quantum yield may be almost 100%, or unattractively low. The desire

* Author for correspondence.

1) Chemical structures are shown in Fig. 1.12.

to understand these and many other photophysical properties developed as the focal point of several research groups, and led to the investigation of these luminescent materials in greater detail. Indeed, the main subject of this chapter is to present the background for an understanding of these emission properties. This will be achieved first by discussing some relatively simple – and, with respect to the number of the involved states, sometimes even slightly oversimplified – models, in order to help to introduce also non-specialists to this field. In later sections, a more detailed description of the photophysics of the triplet state is developed. The discussion of these models, and their relationship to the observed properties, will be outlined in rather elementary terms, and illustrated by examples related to OLED emitter materials. In this respect, references relating to further studies will be given.

This chapter is organized in the following manner. Following a very brief introduction into the working principle of an OLED, exciton formation and the process of electron–hole recombination are addressed. There follows a discussion of the process leading to the population of higher excited singlet and triplet states of the doped emitter molecules, and it is shown, how finally the excitation energy is harvested in the emitting triplet state (Section 1.2). Usually, the same state can be populated either directly or indirectly by photoexcitation; therefore, electroluminescence and photoluminescence spectra result from the same electronic state(s) and thus are normally almost equal, at least for doped triplet emitters in the absence of host emission. Consequently, detailed photoluminescence studies can be applied to explore also the electro-luminescence properties of OLEDs. In Section 1.3, the different types of electronic HOMO–LUMO transitions[2)] are introduced, which are important for organo-transition metal complexes. In particular, ligand-centered (LC), metal-centered (MC), and metal-to-ligand charge transfer (MLCT) transitions are discussed. Models that are based merely on these transitions, however, do not display energy states, such as singlets and triplets. It is possible to show, in a very simple approach, how these states and the related splittings can be deduced from experimentally supported "rules of thumb". More accurate approaches and models, which include SOC, will also be discussed. The emitting triplet state splits almost in any case into three substates. The extent of this splitting – the zero-field splitting (ZFS) – may serve as a very useful parameter for a classification of the corresponding compound, also with respect to its suitability for OLED application. Especially, it will be shown that the magnitude of ZFS depends on the MLCT character in the emitting state, and is governed by SOC. Interestingly, the SOC routes are distinctly different for quasi-square planar as compared to quasi-octahedral complexes. These differences have direct influences on the properties of the emitting triplet state, and thus also on OLED applications. In Section 1.4, an ordering scheme is presented for triplet emitters based on the amount of ZFS, and trends are discussed, how photophysical properties are

2) HOMO = highest occupied molecular orbital; LUMO = lowest unoccupied molecular orbital.

related to the magnitude of the ZFS. In Sections 1.5 and 1.6 it is shown, in a number of case studies applied to $Pt(thpy)_2$ and $Ir(ppy)_3$, how triplet energy level schemes and the emission decay times of the individual triplet substates can be elucidated from highly resolved and broadband emission spectra, respectively. Phosphorescence dynamics and the effects of spin–lattice relaxation (SLR) are addressed in Section 1.7. The influence of high external magnetic fields on the triplet state splitting and the decay dynamics is discussed in Section 1.8, again as a case study focusing on $Ir(btp)_2(acac)$. In Section 1.9, the importance of vibronic coupling is discussed – that is, the origin of the vibrational satellite structure – which is induced by Franck–Condon (FC) and/or Herzberg–Teller (HT) activity, and which usually determines the form and width of an emission spectrum. Finally, in Sections 1.10 and 1.11, environmental effects on the triplet state energy, splitting and decay dynamics are addressed, and spectral broadening by inhomogeneous as well as by homogeneous effects are discussed. The latter effect leads to the unresolved spectral band structure at ambient temperature. These discussions are again based on case studies applied to $Pt(thpy)_2$ and $Ir(btp)_2(acac)$. At higher temperatures, the emission generally represents a thermalized decay from the different triplet substates. In particular in Section 1.11, it is shown that it is possible to simulate the ambient temperature broadband luminescence spectra by use of the well-resolved, low-temperature spectra simply by taking basic spectral broadening mechanisms into account. The chapter is completed with a short conclusion (Section 1.12).

1.2
Electro-Luminescence and the Population of Excited States

In this section, we first present the basic principle of an OLED. Following this short introduction, attention is focused on the energetics and dynamics of electron–hole recombination in the emission layer (EML). Here, the main interest is in those processes which take place within the vicinity of the emitting center. In this context, we explain concepts of exciton formation, spin-statistics, intersystem crossing, and population of the lowest triplet substates, which is often referred to as triplet harvesting.

1.2.1
Multilayer Design of an OLED

Figure 1.1 shows a typical and well-established set-up of an OLED. It consists of a number of thin layers which are either solution-processed or vacuum-deposited, for example, on a glass substrate. In operation, holes are injected from a transparent anode, mostly consisting of a non-stoichiometric composite of SnO_2 (10–20%) and In_2O_3 (90–80%), called “indium tin oxide” (ITO). Adjacent to this anode layer, a hole injection/transport layer (HTL) is normally applied to allow for a well-

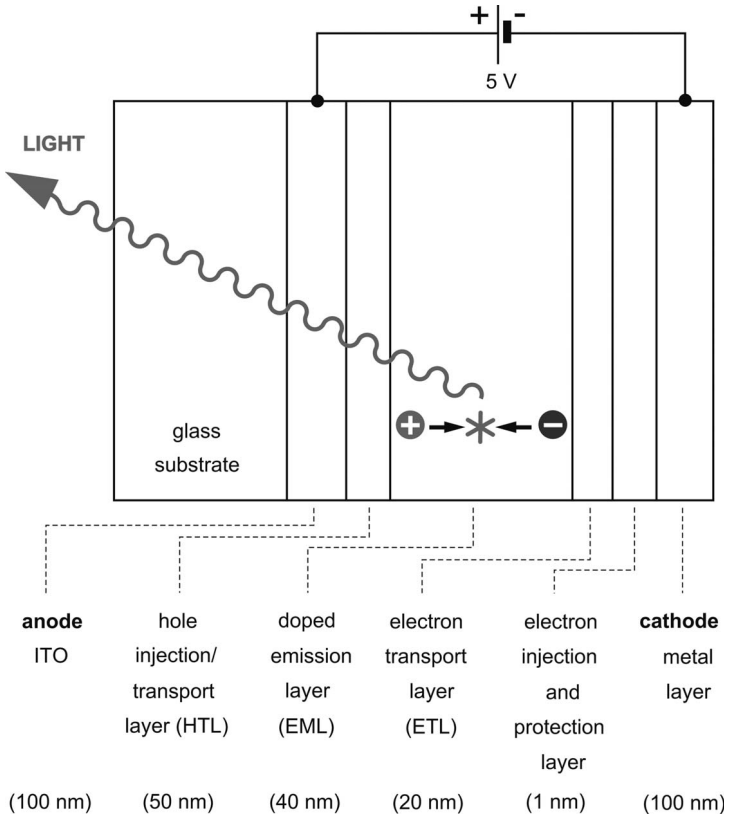

Fig. 1.1 Basic set-up of an organic light-emitting diode (OLED). The different layers are not drawn to scale. Examples of materials used for a realization of an OLED device are given in Fig. 1.2. Within the scope of this chapter, interest is mainly focused on the process of electron(–)–hole(+) recombination and the triplet state population of the emitter molecule (depicted as a star). Further optimized OLEDs contain additional hole and/or electron blocking layers (e.g., see Ref. [42]).

balanced hole[3)] transport into the EML. At the opposite side, a metal-cathode with a suitably chosen work function injects electrons into an electron transport layer (ETL). It has been shown that an additional, very thin layer of LiF or CsF (0.5 to

3) Note that the "hole" represents a model particle which is physically based on the movement (hopping) of an electron. The HOMO of a neutral organic molecule is usually populated with two electrons. If one electron is extracted, for example, by transferring it to the anode, a positively charged molecule is left. Subsequently, the empty electron position in the HOMO can be populated by an electron from the HOMO of a neighboring molecule. Thus, the positive charge has moved to the neighbor. An equivalent process occurs involving the next nearest neighbor, and so on. Thus, the positive charge – called a "hole" – moves from molecule to molecule into direction of the cathode. Such a hole has properties of a particle, it carries a positive charge, a spin (the one of the residual electron) and it can move in the HOMOs with a specific hole mobility. For two molecules with different HOMO energies, the electron hops downwards, and this corresponds formally to an upwards hopping of the hole.

1 nm) strongly reduces the injection barrier and also protects the ETL from chemical reactions with the cathode material [41]. Clearly, although electron transport from the cathode to the EML must be efficient, it is also important that the electron current is well balanced with the hole current in order to avoid ohmic losses. Such losses can be minimized by introducing a hole-blocking layer (e.g., [8, 42]) between the EML and the ETL and/or an electron blocking layer (e.g., [43]) between the HTL and the EML. These additional layers (which are not shown in the diagram) prevent holes/electrons from crossing and leaving the EML without electron–hole recombination. As result, the device efficiency can be distinctly increased. However, such blockings may lead to the build-up of high charge densities at the interfaces, with unfavorable consequences for the device lifetime [44].

The materials used for an OLED device must fulfill a series of requirements, such as suitability for a specific fabrication procedure (e.g., spin-coating, inkjet printing, vacuum deposition), good film-forming properties, sufficiently high glass transition temperature to avoid crystallization of the layer material within the desired lifetime of the device, and chemical and photochemical stability. Moreover, hole and electron injection barriers must be low, and the mobilities as well as HOMO and LUMO energies must match for neighboring layers. A further requirement is that the lowest triplet state of the host material used for the EML lies significantly higher (i.e., about $3000\,cm^{-1}$ or approximately 0.4 eV) than the triplet of the emitting complex. Otherwise, the triplet of the host can be populated, and subsequently the excitation energy can easily diffuse to quenching sites, or can be quenched at the host itself. (Compare also the other contributions to this volume [9, 10]). In particular, for high-energy blue emitters, specific matrix materials must be chosen, or even must still be developed.

Figure 1.2 illustrates one example of a device realized according to the structure depicted in Fig. 1.1. This example (which is adapted from Ref. [45]) is built up by the use of small-molecule, vacuum-depositable materials. The figure depicts the corresponding HOMO und LUMO levels in the absence of an electrical bias, as well as the chemical structures of the materials applied. The diagram shows that energy barriers occur since the hopping of holes upwards (in energy) and of electrons downwards to the EML do not seem to be favored, although this would be advantageous. The energy barriers can be overcome, however, by level shifts due to the external potential, and additionally by thermal activation processes. Level shifts induced by the external potential are not shown in Fig. 1.2. Such a device was first reported by the Forrest and Thompson groups [45] in 2001. It exhibits a relatively high external quantum efficiency of 19% and a luminous power efficiency of $60\,lm\,W^{-1}$. These values are obtained only at low current densities. With increasing currents, the efficiency gradually decreases due to a growing influence of different quenching effects [46], of which triplet–triplet annihilation is regarded as being of particular importance [45–47]. In more recent developments, much higher efficiencies have been obtained with modified devices. For example, by p-doping of the HTL and n-doping of the ETL and additionally by introducing a double emission layer (D-EML), the Leo group [48] obtained with the green-emitting $Ir(ppy)_3$ a luminous power efficiency of $77\,lm\,W^{-1}$ and an external quantum

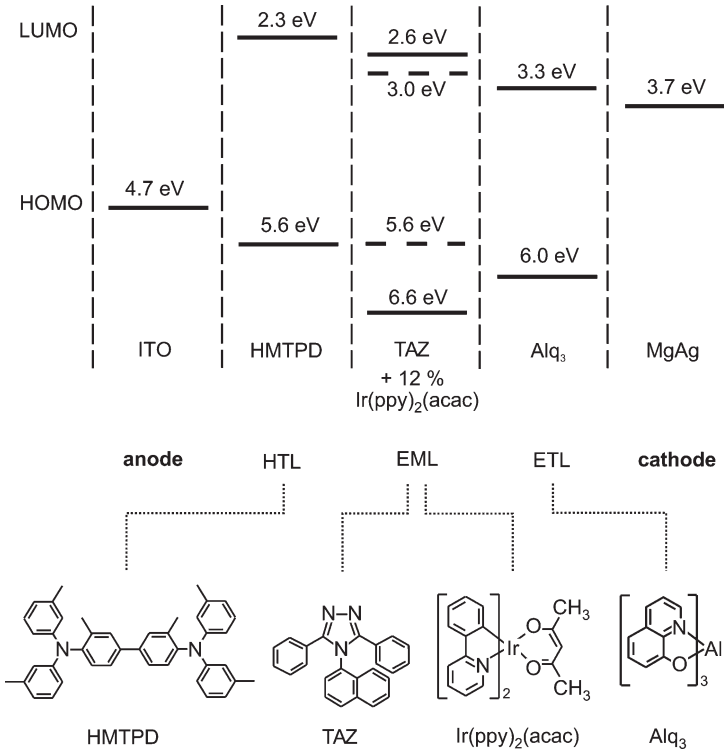

Fig. 1.2 HOMO-LUMO diagram and materials of an OLED device similar to the one shown in Fig. 1.1. The HOMO/LUMO values are given relative to the vacuum level, and therefore are negative. Values and materials are taken from Ref. [45]. For the emission layer (EML), the oxidation and reduction potentials are given for the host (TAZ, solid line) and the emitter ($Ir(ppy)_2(acac)$, dashed line).

efficiency of more than 19% at $100\,cd\,m^{-2}$ at an operating voltage of only 2.65 V. Also applying the $Ir(ppy)_3$ complex, the authors of Ref. [49] obtained a luminous power efficiency of $79\,lm\,W^{-1}$ and a current efficiency of $81\,cd\,A^{-1}$ by use of a transparent silver anode. This device structure features an enhanced hole injection, and also allows for more efficient outcoupling of light due to a microcavity structure. In Ref. [50], values of $110\,lm\,W^{-1}$ at $10^3\,cd\,m^{-2}$ were communicated. By use of a microcavity, two-unit tandem device, efficiencies as high as $200\,cd\,A^{-1}$ at $10^3\,cd\,m^{-2}$ were reported recently [51]. Interestingly, efficiencies which can be reached today with OLEDs are as high as – or even higher than – those of highly efficient inorganic LEDs.

Although, in this chapter, we do not aim to discuss further progress in the field of OLED device architectures, it is referred to some interesting recent developments reported in the literature [51–60].

1.2.2
Electron–Hole Recombination, Relaxation Paths, and Light Emission

In order to gain some general understanding of the processes in the EML, Fig. 1.3 displays a simplified model of electron–hole recombination. This layer consists of a host material (matrix) which is doped with a suitable triplet emitter complex at low concentration. For the subsequent discussion, it is assumed that both charge carriers – electron and hole – are already present in the EML. Different steps of electron–hole recombination – that is, exciton formation and population of the emitting triplet state – can take place. For example, the exciton can be formed and trapped on the host molecule with subsequent energy transfer to the triplet emitter. In an alternative process, one of the charge carriers is directly trapped on the emitter dopant itself and the recombination occurs on this molecule. This has been proposed specifically for efficient devices containing Ir(III) emitter complexes [45, 61, 62], but also for PtOEP [63], that the hole is trapped first on the emitter complex. The electron – or, more exactly, the negatively charged polaron[4)] [64] – experiences a Coulomb attraction and the formation of the overall neutral exciton starts. This process of hole trapping as a first step can occur, if the oxidation potential of the emitter complex fits well to the HOMO energy of the hole transport material (HTL) (compare Ref. [45]). Presumably, this process of charge carrier trapping directly on the emitter molecule will usually result in a more efficient OLED device than by indirect excitation of the emitter molecule by energy transfer [5]. In part, alternative approaches for the description of exciton formation processes are discussed in Refs. [5, 65, 66].

For the model depicted in Fig. 1.3, it is assumed (as mentioned above) that the hole is already trapped at the emitter molecule. In our simple approach, it is supposed that the reorganization energy after oxidation of the emitter (hole trapping) sitting in the relatively rigid host environment is small. Subsequently, we discuss the electron dynamics until the emitting triplet state is populated. With an external potential ΔV, the electron will migrate through the host material towards the anode. Under normal conditions, this process additionally requires thermal activation energy to overcome energy sinks due to inhomogeneities and due to host reorganization effects related to the polaronic properties of the electron. Electron trapping is avoided if the energies of the sink depths are less than, or on the order of, the thermal energy $k_B T$, where k_B is the Boltzmann constant and T the absolute temperature.

When the electron is still far from the trapped hole, it will migrate towards the anode independently from the hole. Thus, the hole and electron are neither bound nor correlated (see left-hand side of the diagram, Fig. 1.3). However, when the electron migrates further into a region given by a critical electron–hole separation R_C, the positively charged hole (h) will attract the electron (e). This distance is

4) Electron (or hole) hopping is normally connected with a polarization of the matrix. Therefore, the corresponding negatively (positively) charged particle coupled to matrix distortions represents a polaron. For background information see, for example Ref. [64].

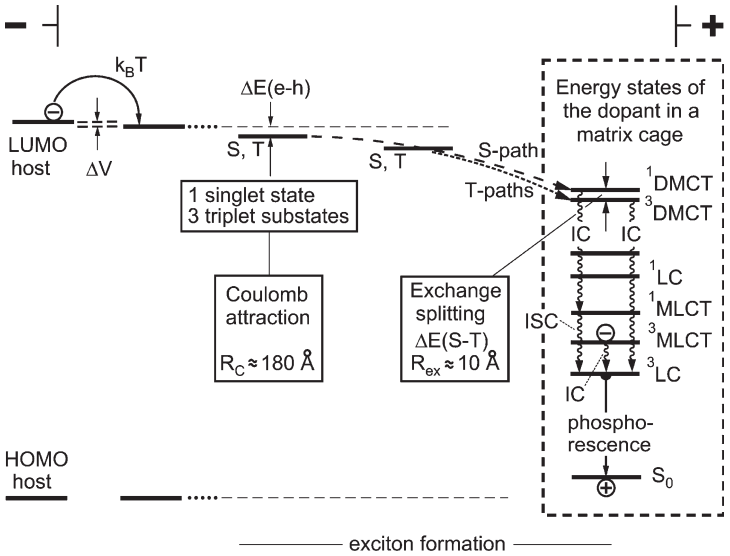

Fig. 1.3 Dynamics of exciton formation. In this model, the exciton formation is induced by Coulomb attraction between electron and hole and starts already at a separation of 150 to 180 Å. The exciton trapping on the emitter complex, which is doped into a host material, occurs via charge transfer states [5, 69]. The wavefunctions of these **^{1,3}DMCT** states extend over 10 to 15 Å, and thus involve the triplet emitter itself and the nearest-neighbor host molecules. The exciton trapping processes lead finally to the population of the lowest excited triplet state(s) of the emitter molecule via internal conversion (IC) and intersystem crossing (ISC). The lower-lying states depicted in the dashed frame represent electronic states of the doped emitter molecule itself. Note, this energy level diagram is strongly simplified.

reached when the energy of Coulomb attraction $\Delta E(e-h)$ is of similar size as the thermal energy $k_B T$. Thus, for an estimate of R_C, we can write

$$\Delta E(e-h) = \frac{e^2}{4\pi\varepsilon_0\varepsilon R_C} = k_B T \tag{1}$$

wherein e is the electron charge and ε_0 and ε represent the dielectric constants of the vacuum and the host material, respectively. If a dielectric constant of $\varepsilon = 3$ is assumed, a value of $R_C \approx 180$ Å is obtained for $T = 300$ K. This means that the electron experiences the hole potential even when it is still far from the trapped hole. Both particles are already bound, although a relatively large number of host molecules lies between electron and hole. These two attracting particles may already be called "exciton". However, at this electron–hole separation, the exciton can easily dissociate thermally.

For the further discussion, it is required to take also the spins of both electron and hole into account. The spin of the hole is given by the spin of the residual electron at the emitter molecule. In a quantum mechanical treatment, in which

the bound electron–hole states must be described by four antisymmetrized wavefunctions, the spins are coupled and *four* new combined states are obtained – that is, *one* singlet state and *one* triplet state. The triplet consists of *three* substates. These substates differ from each other mainly by their relative spin orientations. An energy splitting between the resulting singlet and triplet states may be neglected at large electron–hole separations. Therefore, the corresponding exciton state – being four times quasi-degenerate – is shown in Fig. 1.3 (middle) just by one energy level, designated as **S**, **T**. In a statistical limit, all *four* substates of this exciton state will be formed (populated) with equal probability. Consequently, a *population ratio of one to three* of singlet to triplet substates is obtained. For a more detailed discussion concerning the statistically determined population ratio, see Refs. [67, 68].

Driven by the long-range electron–hole Coulomb attraction, the electron moves further on matrix molecules towards the trapped hole. When the electron reaches a distance of 10 to 15 Å – that is, when the electron is approximately located in the first coordination sphere of the emitter dopant – the wavefunctions of electron and hole (or that of the residual electron) begin to overlap slightly [5, 69]. Consequently, the exchange interaction must be taken into account. This quantum mechanical interaction, based on the electron–electron interaction, is responsible for a splitting $\Delta E(S-T)$ of the singlet state **S** and the triplet state **T** by about twice the exchange integral. In this situation of small wavefunction overlap, $\Delta E(S-T)$ depends approximately exponentially on the electron–hole separation R

$$\Delta E(S-T) \sim \exp(-aR) \tag{2}$$

where a is a constant which depends on the individual wavefunctions of the emitter dopant and the nearest neighbor host molecules. Due to the still relatively large electron–hole separation of 10 to 15 Å with respect to the extension of the wavefunctions, the singlet–triplet splitting is expected to be very small, i.e. much smaller than is typically found for singlet–triplet splittings in molecules.

In the subsequent discussion, we follow further the model first presented by Yersin [5, 69]. According to this approach, it is suitable to analyze the above-described situation also from a slightly different viewpoint. Let us focus only on the emitter complex, the dopant (D), and its first coordination sphere of matrix (M) molecules. In this relatively large dopant–matrix–cage unit, the hole is located in the HOMO of the dopant and the electron resides on the LUMO of a matrix molecule. This situation corresponds to a charge transfer excitation. The corresponding states represent dopant-to-matrix charge transfer (DMCT) states. When the spin of the remaining electron in the HOMO of the dopant (D) and the spin of the electron in the LUMO of the matrix (M) molecule as well as the electron–electron interaction are taken into account, ^{1}**DMCT** and ^{3}**DMCT** states are obtained.[5)] The corresponding splitting is relatively small due to the weak overlap

5) In Section 1.3, we will discuss in more detail, how singlet and triplet states are deduced from HOMO–LUMO excitations.

of the involved molecular orbitals. Clearly, these two states correspond to those exciton states **S** and **T** which are realized at a small electron–hole separation (Fig. 1.3).

The discussion presented above allows us to relate the exciton states with states of a larger molecular unit which consists of the dopant and its matrix cage. This molecular unit exhibits the ^{1}**DMCT** and ^{3}**DMCT** states as well as a number of lower-lying states which are largely confined to the dopant (triplet emitter) itself, such as $^{1,3}\pi\pi^*$, ^{1,3}**dd***, ^{1,3}**MLCT** states or adequate mixtures of these (see also Section 1.3).[6)] The resulting energy level diagram is depicted in the dashed frame of Fig. 1.3.

Interestingly, on the basis of this energy level scheme, one obtains also information about the relaxation paths from the exciton charge transfer states ^{1}**DMCT** and ^{3}**DMCT** to the lower-lying states which largely belong to the emitting center. In particular, the relaxation from the ^{1}**DMCT** state to lower states will be faster within the system of singlet states than making a spin-flip first. This is due to the fact that SOC in organic host molecules (matrix) is relatively small and, thus, intersystem crossing (ISC) is not favored. As consequence, a fast singlet path (internal conversion) is obtained that finally populates the lowest singlet state (Fig. 1.3). Subsequently, the population of this lowest singlet will be followed by ISC processes to the lowest triplet substates. In case of significant singlet–triplet mixing due to SOC, the difference between ISC and internal conversion (IC) might be lost. An initial population of the ^{3}**DMCT** state is similarly followed by a very fast relaxation (IC) within the system of triplet states down to the lowest triplet state (Fig. 1.3). The beginning of these relaxation processes corresponds to the singlet and triplet paths in the exciton trapping model, as shown in Fig. 1.3 (compare Refs. [5, 69].) The relaxation times within the singlet and triplet system, respectively, are of the order of 1 ps or faster, while the ISC processes can be slower or of similar time, depending on the importance of SOC and the resulting perturbation of the lowest triplet by singlet admixtures. In a favorable situation, which is usually realized for the organo-transition metal triplet emitters, the ISC rate is very high (order of 10^{12} to $10^{13}\,s^{-1}$) [70, 71]. Thus, relaxation processes to the lowest triplet state occur mostly with a yield of 100%. This means that all originally formed singlet excitons (25%) and triplet excitons (75%) finally relax into the lowest triplet state of the doped emitter molecule. This process is called *triplet harvesting*. Therefore, under suitable conditions a fourfold larger electro-luminescence efficiency for triplet emitters can be obtained compared to purely organic singlet emitters.[7)]

6) Within this simple model, it is assumed that the energy states of the matrix (host) molecules lie at relatively high energies and thus do not interfere significantly with the lower-lying states of the dopant (triplet emitter).

7) For purely organic molecules, the radiative triplet–singlet transition rates are, at ambient temperature, orders of magnitude smaller than the corresponding non-radiative rates. Therefore, any excitation energy is converted into heat and the triplets do not emit.

1.3
Electronic Excitations and Excited States

In general, photoluminescence properties are largely determined by the nature of those molecular orbitals (MOs), which are mainly responsible for the electronic ground state and the lowest excited state. These are called "frontier orbitals". Here, the aim is to focus on organo-transition metal complexes, such as $Ir(ppy)_3$, $Ir(ppy)_2(CO)(Cl)$, $Ir(btp)_2$ (acac), $Pt(thpy)_2$, $[Pt(bpy)_2]^{2+}$, $Re(phen)(CO)_3(Cl)$, $[Ru(bpy)_3]^{2+}$, $[Os(bpy)_3]^{2+}$, etc. For such compounds, different excitations between various MOs have to be taken into account.[8] Specifically, there are

- ligand-centered (LC) excitations, e.g., of π-π^* character
- metal-centered (MC) excitations, e.g., of d-d* character
- metal-to-ligand charge transfer (MLCT) excitations, e.g., of d-π^* character.

In these descriptions, the asterisk refers to an excited (i.e., a non-occupied) MO.

However, it is not sufficient to restrict the discussion only to HOMO $\leftrightarrow$ LUMO transitions. Energetically nearby lying orbitals can also dominate emission properties. Thus, HOMO-1, HOMO-2, LUMO+1, LUMO+2, etc. have also to be included in the set of frontier orbitals. In this section, we discuss properties of the above-mentioned excitations and trends concerning the resulting electronic states, such as singlet and triplet states. These are many-electron states and can be significantly mixed by SOC. This presentation will initially be carried out using rather simple models, although more detailed descriptions are also presented later on to illustrate the nature of the set of low-lying states and the importance of SOC.

1.3.1
Ligand-Centered (LC) Transitions: States and Splittings

In a series of compounds, the lowest excited states are determined dominantly by MOs which can be well described by the π-HOMO and the π^*-LUMO of the organic ligands, since MOs of other than π and π^* character lie at significantly lower and higher energies, respectively. Thus, it is suitable to confine a first-order approach only to the HOMO-LUMO excitation(s) of the ligand(s). Clearly, these orbitals and their energies are somewhat altered by coordination of the ligand(s) to the positively charged metal. Usually, this leads to a red shift (i.e., a shift to lower energy) of the corresponding transitions of the order of $10^3\,cm^{-1}$ ($\approx$0.12 eV).[9] Of course, the metal induces further changes, and in particular changes which

8) For completeness, also ligand-to-metal-charge-transfer (LMCT) excitations, e.g., of π-d* character, are mentioned. However, for the compounds of interest in this chapter the corresponding excited states exhibit relatively high energies and therefore, are not discussed at this point.

9) $1\,eV \triangleq 8068\,cm^{-1}$.

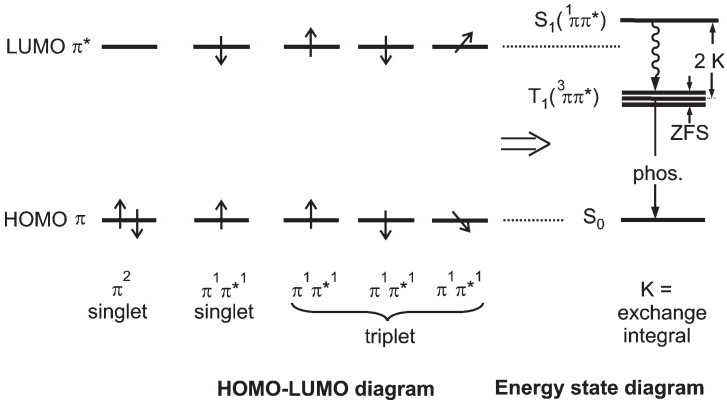

Fig. 1.4 Comparison of a HOMO-LUMO diagram to an energy state description. The configuration π^2 leads to the ground state $\mathbf{S_0}$, while the configuration $\pi^1\pi^{*1}$ gives four different excited states, one singlet $\mathbf{S_1}$ and one triplet $\mathbf{T_1}$ which consists of three substates. By taking the change of electron–electron interaction for both configurations into account, usually a significant $\Delta E(S_1 - T_1)$ splitting is obtained. For ligands which are in the focus of this contribution, $\Delta E(S_1 - T_1)$ can be as large as $10^4\,cm^{-1}$. The three triplet substates of $\mathbf{T_1}$ exhibit a splitting, the zero-field splitting (ZFS). The corresponding value can be used to assess a triplet emitter compound for its application in an OLED. (See Section 1.4 and Fig. 1.11.)

result from SOC, such as changes of radiative and non-radiative rates as well as of energy splittings. (These important effects will be discussed later in Sections 1.3.3.3 and 1.4.2.) For completeness, it should be mentioned that, for this class of compounds, the lowest excited state (the triplet state) is largely localized on one ligand (compare Refs. [72–74] and Section 1.4.2).

For most molecules, which are of interest here, the HOMO is occupied by two electrons and the compound is diamagnetic. Thus, the two electrons carry opposite spins (α and β spins). This situation is described by an electron configuration of π^2. The resulting state, the ground state, is a spin singlet $\mathbf{S_0}$ ($^1\boldsymbol{\pi}^2$) (Fig. 1.4, left). When, after a HOMO–LUMO excitation the spins are also taken into account, one obtains for the excited state configuration $\pi^1\pi^{*1}$ four different situations (Fig. 1.4, middle). An excitation without a spin flip gives an excited singlet, while an excitation with a spin flip gives a triplet due to three different possible spin orientations. This description is similar to the one discussed in Section 1.2.2. Again, in a quantum mechanical treatment, four different (antisymmetrized) wavefunctions must be formulated to describe the resulting singlet and the three triplet states (compare , for example, Ref. [75], p. 163).

In the simple HOMO–LUMO model, all four states, which result from the $\pi^1\pi^{*1}$ configuration, still have the same energy and are degenerate. However, from spectroscopic investigations it is known that the splitting between the excited singlet state and the excited triplet state is usually significant. For example, for the ligands discussed in this chapter, it can be as large as $10^4\,cm^{-1}$ (≈1.24 eV). There-

fore, the HOMO–LUMO model must be improved, specifically, by taking changes of the electron–electron interaction into account which are connected with the HOMO–LUMO excitation. This results in the energy state diagram (or the many electron state diagram) as depicted in Fig. 1.4 (right-hand side). A quantum mechanical consideration shows that the triplet state $\mathbf{T}_1$ (or $^3\boldsymbol{\pi\pi^*}$), consisting of three substates, is stabilized by an energy given by a difference of Coulomb integrals, while the singlet state $\mathbf{S}_1$ (or $^1\boldsymbol{\pi\pi^*}$) is destabilized relative to the triplet state by twice the exchange integral

$$K = \text{const} \times \left\langle \pi(r_1)\pi^*(r_2) \left| \frac{1}{r_{12}} \right| \pi(r_2)\pi^*(r_1) \right\rangle \tag{3}$$

wherein π and π^* are the HOMO and LUMO wavefunctions, r_1 and r_2 represent the electron coordinates, and r_{12} the separation between the two electrons (compare, for example, Ref. [75], p. 174). The exchange interaction is a quantum mechanical effect which takes the spin correlation into account. This means that two electrons with opposite spin orientations (in the singlet state) have a larger probability of being found near to each other than two electrons with the same spin orientation (the triplet state). In the latter situation, the two electrons have the tendency to avoid each other. Hence, the average electron–electron repulsion is smaller and thus the triplet has a lower energy than the singlet state (Fig. 1.4).

The exchange integral – as displayed in Eq. (3) in a shortened notation (compare, for example Ref. [76]) – is given in this elementary chapter, since it permits important qualitative conclusions to be reached by considering the overlap of the involved wavefunctions. The following conclusions fit to the spin correlation model discussed above. First, with an increasing conjugation length of the π and π^* orbitals, the exchange integral K becomes smaller. For example, in purely organic molecules, the singlet-triplet splitting $\Delta E(^1\pi\pi^* - {}^3\pi\pi^*)$ decreases in the series of benzene, naphthalene, anthracene from $\approx 18\,000\,\text{cm}^{-1}$ ($\approx 2.2\,\text{eV}$) [77], to $12\,300\,\text{cm}^{-1}$ ($\approx 1.5\,\text{eV}$) [78], and to $10\,500\,\text{cm}^{-1}$ ($\approx 1.3\,\text{eV}$) [78]. Second, when the MOs are mainly confined to different spatial regions of the molecule, the MO overlap can become very small, and consequently so also can the integrals. For example, for *n*-HOMO to π^*-LUMO excitations, which are relevant for organic molecules with heteroatoms, such as benzophenone, the singlet-triplet splitting $\Delta E(^1n\pi^* - {}^3n\pi^*)$ amounts to only $1750\,\text{cm}^{-1}$ ($\approx 0.22\,\text{eV}$) [79]. Equivalent considerations apply also to states of organotransition metal complexes. Small admixtures of metal d-orbital or MLCT character to the ligand-centered states will increase the spatial extension of the wavefunctions and thus reduce the exchange integral – that is, the singlet–triplet splitting between the perturbed $^1\mathbf{LC}(^1\boldsymbol{\pi\pi^*})$ and $^3\mathbf{LC}(^3\boldsymbol{\pi\pi^*})$ states. For example, $\Delta E(^1\pi\pi^* - {}^3\pi\pi^*)$ of the free ligand H(2-thpy) is of the order of $10^4\,\text{cm}^{-1}$ (1.24 eV), as can be estimated from the data given in Ref. [80], whereas for $Pd(thpy)_2$ (doped into *n*-octane) $\Delta E(^1LC - {}^3LC)$ is significantly smaller and amounts only to $5418\,\text{cm}^{-1}$ [70]. This tendency becomes even more obvious for $^1\mathbf{MLCT} - {}^3\mathbf{MLCT}$ splittings.

The triplet state is always split into three substates, at least, if the symmetry of the molecule is sufficiently low.[10] This is valid for most organo-transition metal compounds that are of interest for OLED applications. The splitting occurs also at zero magnetic field, and is therefore referred to as zero-field splitting (ZFS) (Fig. 1.4). For $^3\pi\pi^*$ states of organic molecules, the ZFS is mainly induced by spin–spin interactions of the two unpaired electrons in the triplet state (compare, for example, Refs. [77, 81, 82]). This interaction leads to ZFS-values of the order of $0.1\,cm^{-1}$ ($\approx 1.2\times10^{-5}$ eV). For largely ligand-centered ^{3}**LC** states of organo-transition metal complexes, the value of ZFS lies in the same order of magnitude. For example, for $[Rh(bpy)_3]^{3+}$, the total ZFS has been determined as $0.125\,cm^{-1}$ ($\approx 1.55\times10^{-5}$ eV) [83, 84], and for $Pd(qol)_2$ to about $0.25\,cm^{-1}$ ($\approx 3.1\times10^{-5}$ eV) [85]. However, SOC carried by metal d-orbitals can drastically increase the magnitude of ZFS, as found for ^{3}**MLCT** states. (Compare especially Sections 1.3.3, 1.4, and Refs. [5, 70, 72–74].) In this situation, the small contribution from spin–spin interactions can be neglected.

For completeness it is mentioned that, although the ZFS values of only slightly perturbed ^{3}**LC**($^3\pi\pi^*$) states of organo-transition metal compounds are of similar size, as found for purely organic molecules, the metal can manifest itself already drastically by increasing radiative and/or non-radiative rates. This is a consequence of a relatively small but still very effective SOC. For instance, the population of the triplet from an excited singlet state by ISC becomes orders of magnitude faster. Thus, the quantum efficiency of ISC reaches 100%. For example, for $Pd(thpy)_2$ [70] and $Pt(qol)_2$ [86], which both emit from ^{3}**LC** states, we determined ISC relaxation times of $\tau(ISC) = 800$ fs and 500 fs, respectively. Moreover, the radiative $\mathbf{T_1} \rightarrow \mathbf{S_o}$ rate also becomes orders of magnitude larger than are found for purely organic molecules. Thus, mostly the triplet substates can easily be excited resonantly [87, 88].[11] This implies that the increased radiative rate can dominate over the non-radiative deactivation. As a consequence, even high-emission quantum yields can occur. For example, for $Re(phbt)(CO)_4$ – a ^{3}**LC**($^3\pi\pi^*$) emitter with a ZFS much smaller than $1\,cm^{-1}$ – the photoluminescence quantum yield ϕ_{PL} amounts to 27% at ambient temperature in ethanol (Ar saturated) [88]. However, the emission decay time of $\tau(300\ K) = 21\,\mu s$ is still relatively long, and therefore the compound is probably not well suited for OLED applications [88] but probably well suited as an oxygen sensor molecule. It will be shown below that the size of ZFS represents a good measure of the importance of MLCT character in the lowest triplet state and that, for the most efficient OLEDs, emitter compounds are used which exhibit

10) Molecules which belong to a point group symmetry lower than C_3 do not exhibit any state degeneracies (apart from Kramer's degeneracies of molecules with uneven numbers of electrons).

11) For several compounds only two of the three triplet substates of dominant ^{3}**LC** character can be excited directly from the ground state, while the transition to the third substate is still largely forbidden. This has, for example, been shown for $Pd(thpy)_2$ [70], $Pt(qol)_2$ [71], $Ir(ppy)_2(CO)(Cl)$ [87], and $Re(phbt)(CO)_4$ [88].

ZFS-values of about 10 cm^{-1} or larger (1.2×10^{-3} eV). (Compare Sections 1.3.3, 1.4, and Refs. [5, 70, 72–74].)

1.3.2 Metal-Centered Transitions and States

A large number of compounds is known, for which the absorption and luminescence properties are determined by metal-centered (MC) excitations. For example, complexes or doped materials of main-group metal ions with s^2 ground state and sp excited state configurations have low-lying MC excitations (e.g., $[PbCl_4]^{2-}$) [89–91]. Lanthanide compounds with f-f excitations also exhibit MC transitions (e.g., Eu^{3+}, Tb^{3+} compounds; see e.g., Refs. [92–96]). A short summary of compounds which exhibit different types of MC transitions is found in Ref. [91]. However, within the scope of the present chapter, we are interested in properties of d-d* excitations and related states. Well-known compounds with optical properties dominated by such MC excitations include ruby (Cr^{3+} in Al_2O_3) [97, 98]) and $[Cr(urea)_6]^{3+}$ [99–101], both with $3d^3$ configurations. The latter compound is among the first synthesized transition metal complexes with organic ligands. Further examples include $[MnCl_4]^{2-}$ [102], $[Co(CN)_6]^{3-}$ [103, 104], and $[PtCl_4]^{2-}$ [104, 105], in which the metal centers have $3d^5$, $3d^6$, and $5d^8$ configurations, respectively.

The d-orbitals and d-d* transitions are indirectly of importance for OLED materials. This is due to two different effects. On the one hand, the quantum mechanical mixing of d-orbitals of open-shell transition metal ions, such as Pt^{2+}, Ir^{3+}, or Os^{2+}, can induce the required SOC to make the formally forbidden triplet–singlet transitions sufficiently allowed (see next section). On the other hand, states which result from d-d* excitations often quench the emission efficiently, and therefore should not lie in a thermally accessible energy range of the emitting states (see below).

Usually, a description of dd* states is carried out by use of group theory and the symmetry of the complex. An introduction to ligand field or crystal field theory is found in most inorganic chemistry textbooks (e.g., see Refs. [106, 107]), whilst more detailed descriptions are found in Refs. [108, 109]. At this point, we present only a brief illustration of excitations (in particular of HOMO–LUMO excitations), provide some comments regarding the resulting states, and highlight the relevance of these states for triplet emitters in OLEDs. In this section, only those compounds having central metal ions with a d^6 configuration, such as Ir^{3+}, Ru^{2+}, Os^{2+}, Re^{+}, and W^0, will be discussed as examples. These metals/ions tend to prefer a sixfold coordination which includes, for example, three bidentate chelates. In a first-order approach, the complexes can be described in an octahedral symmetry (symbol: O_h) of the first coordination-sphere around the central metal. In this symmetry, the d-orbitals split into two sets of orbitals (Fig. 1.5). The magnitude of splitting is given by the ligand field strength, and amounts to Δ which is – for historic reasons – often named 10 Dq. The Dq parameter varies with the ligand according to the spectrochemical series (compare , for example Refs. [107], p. 221, and [108], p. 84):

$$J^- < Br^- < S^{2-} < Cl^- \approx \underline{S}CN^- < N_3^- < (C_2H_5O)_2PS_2^- < NO_3^- < F^-,$$
$$< (C_2H_5)_2NCS_2^- < (NH_2)_2C\underline{O}\ (\text{urea}) < OH^- < C_2O_4^{2-} < H_2\underline{O} < \underline{N}CS^- <$$
$$NH_3 < C_5H_5N < NH_2 - CH_2 - CH_2 - NH_2 \approx SO_3^{2-} < NH_2OH < \text{bpy} <$$
$$\text{phen} < NO_2^- < PPh_3 < CH_3^- \approx C_6H_5^- < ppy^- < \text{carbene}^- < CN^- < CO$$

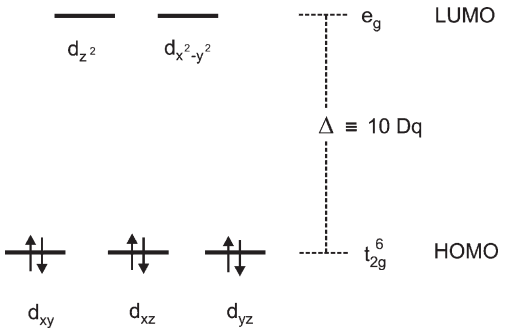

Fig. 1.5 Splitting of d-orbitals in an octahedral ligand field with O_h symmetry. For a high ligand field (large Δ or Dq value), the ground state configuration is t_{2g}^6.

This series gives the approximate ordering of the Dq parameter.[12)] In particular, ligands found on the left-hand side induce a small ligand field splitting (they are called "weak" ligands), while those on the right-hand side of the series are "strong" ligands with large ligand field splittings. These splittings depend also on the central metal ion. For OLED applications, one is usually interested in compounds with large ligand field splittings to avoid emission quenching processes at ambient temperature (see below). Consequently, it is useful to have some rules of thumb for the development of efficient triplet emitters. Such rules should help to estimate changes of Dq values with chemical variations. Indeed, if a reference compound is available, then specific trends can be given (Ref. [108], p. 83):

1. Compounds with the same ligands and the same central metal ion exhibit a 40–80% Dq increase, when the metal oxidation changes from 2+ to 3+.
2. Compounds with the same ligands experience an increase of Dq by 30–40%, when the metal of the first row of transition metal ions in the Periodic Table is replaced by one of the second row, and similarly if a second-row metal ion is replaced by one of the third row.
3. For compounds with mixed ligands (heteroleptic compounds), the Dq value can be estimated from the average ligand field strength.

12) According to different binding properties in different complexes, the sequence of the ligands in the spectrochemical series may slightly vary. In particular, the positions of $(ppy)^-$ and carbenes$^-$ are given only tentatively.

From Fig. 1.5 it is clear that compounds with a d^6 electron configuration and a large ligand field splitting have a t_{2g}^6 ground state configuration (in an O_h parent group approach). Thus, the t_{2g} sub-shell is filled. This leads to a low-spin compound with a (totally symmetric) diamagnetic ground state ($^1A_{1g}$ in O_h). From the excitations $t_{2g}^6 \rightarrow t_{2g}^5 e_g^1$ and $t_{2g}^6 \rightarrow t_{2g}^4 e_g^2$ etc., the excited states can be determined by taking electron–electron interaction into account (e.g., see Refs. [108, 109]). Usually, this is carried out by use of group theoretical methods. For example, for the $t_{2g}^5 e_g^1$ configuration, two triplets and two singlets are obtained. In a group theoretical notation (in the O_h group), the terms ordered according to increasing energy are $^3\mathbf{T}_{1g}$, $^3\mathbf{T}_{2g}$, $^1\mathbf{T}_{1g}$, and $^1\mathbf{T}_{2g}$. Further excitations such as $t_{2g}^6 \rightarrow t_{2g}^3 e_g^3$ lead to a number of additional energy states. All of the resulting states are summarized in the well-known Tanabe–Sugano diagrams, which are found in many inorganic textbooks (e.g., see Ref. [106], p. 1189, and Ref. [107], p. 683).

It is an important property that all of these excited states have distinctly larger metal–ligand bond lengths than the ground state. This can simply be deduced by visualizing the effects of the HOMO–LUMO excitation of $t_{2g}^6 \rightarrow t_{2g}^5 e_g^1$. It corresponds to a population of an anti-bonding e_g orbital from a non-bonding t_{2g} orbital. Therefore, the metal–ligand bond lengths increase, and additionally the potential surfaces become less stiff (smaller force constants). Consequently, the potential surfaces of the ground and of the excited states can cross at relatively low energies. These changes can have significant effects on non-radiative deactivation processes. This is due to a resulting distinct overlap of lower-lying vibrational wavefunctions of the excited electronic state with high-energy vibrational wavefunctions of the electronic ground state. Accordingly, the corresponding Franck–Condon factors which govern the rate of the radiationless deactivation from the excited state to the ground state, increase (compare , for example, Refs. [78], p. 71 and [110], p. 129). As consequence, the radiationless deactivation rate can become significantly larger than the radiative rates, and an emission is prevented ("quenched").

In summary, a population of the excited ^{1,3}**dd*** states of transition metal compounds with a d^6 configuration often leads to emission quenching at ambient temperature. Although, for OLED applications, the ^{1,3}**dd*** states do not have to be characterized in detail, it is still required to take care of these quenching states. Energetically, they should not lie too close to the emitting states of, for example, ^{3}LC/^{3}MLCT character (compare next section). An energy difference of 3000 to 4000 cm^{-1} (0.37 to 0.50 eV) is required to obtain a sufficiently small Boltzmann factor, and thus a sufficiently small population of the quenching state, at ambient temperature. Note that arguments similar to those developed for central metal ions with a d^6 configuration also hold for compounds with a d^8 configuration, such as Pt(II) or Ir(I) complexes.

However, a strategy which aims to maximize the ligand field strength in order to shift the ^{1,3}**dd*** states to an energy as high as possible will fail. For a very high Dq value, the occupied d-orbitals may be stabilized too much. This can have the consequence that a necessary MLCT admixture to the emitting triplet becomes too small and that the resulting compound turns into a less effective ^{3}**LC** emitter. Exactly this behavior is observed for Re(I) complexes. $Re(phen)(CO)_3(Cl)$ shows a

relatively good OLED performance [111, 112] which is related to a large ZFS of 50 cm^{-1} and thus to a large MLCT perturbation of the emitting triplet. For $Re(phbt)(CO)_4$, on the other hand, with ligands of an on-average much higher Dq value, the emitting state turns out to be a ^{3}**LC** state (ZFS << 1 cm^{-1}) [88]. For this latter material, only a very weak OLED performance was observed [88]. Obviously, a good balance between MLCT character of the emitting state and a high energy separation of the quenching state must be found.

1.3.3 Metal-to-Ligand Charge Transfer/Ligand-Centered Transitions: States in Organo-Transition Metal Triplet Emitters

In the two previous sections, we have discussed well-seizable models with respect to the frontier orbitals and the resulting energy states. The situation becomes a little more complicated, when additionally MLCT transitions are taken into account. In particular, the interplay – that is, the quantum mechanical mixing between ^{3}**LC**, ^{1}**LC**, ^{3}**MLCT**, and ^{1}**MLCT** states – determines the properties of the lowest triplet state and thus also the applicability of an emitter material in an OLED. For example, a compound with an almost "pure" ^{3}**LC** emitting state would presumably not be well suited as an OLED emitter, whereas a complex with a mixed emitting ^{3}**LC**/^{3}**MLCT** state might be a very good candidate. Such mixtures can occur, for instance, for a d-orbital admixture to the HOMO of mainly π character, that is, for $\pi d \rightarrow \pi^*$ transitions. (Compare the examples given at the end of Section 1.3.2 with those later in this section.) The inherent reason is SOC which, for the compounds under consideration in this contribution, is carried by the metal 5d-orbitals.

It is the subject of this section, to illustrate how many-electron states result from frontier orbitals, such as HOMO-1, HOMO, LUMO, LUMO+1, etc., and to discuss the properties of electronic states, the MLCT character, SOC routes, triplet state splittings, and radiative rates. In a first step (see Section 1.3.3.1.), a very simple model is presented with a strongly restricted number of MOs. Yet, this model is well suited for describing some trends. In a second step (see Section 1.3.3.2.), it will be shown that a more realistic model requires the inclusion of a larger number of active frontier orbitals, and a very large number of states in the optical energy range is obtained. Finally, in Section 1.3.3.3, the important effects induced by SOC are discussed.

1.3.3.1 Introductory MO Model and Energy States

Figure 1.6 illustrates a strongly simplified MO diagram for an organo-transition metal compound, and how the MOs relate to the energy states. In this model, one single ligand π-orbital (HOMO-1) and one d-orbital (HOMO) are considered as the occupied frontier orbitals. Both of these are occupied with two electrons. The lowest unoccupied orbital is given by a single π*-MO. An additional unoccupied d*-orbital, also displayed in the figure, is not further discussed, as it is assumed that its energy and those of the resulting states are sufficiently high and thus have no importance for this introduction (but compare Section 1.3.2). In summary, this

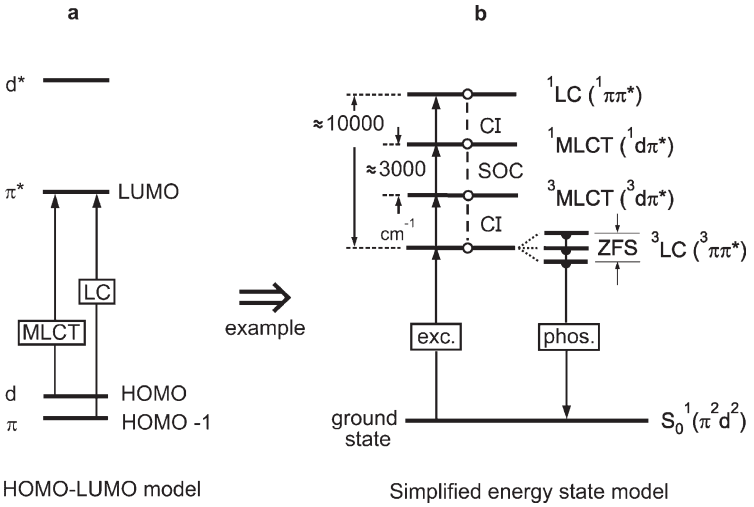

Fig. 1.6 (a) Introductory MO model for a compound with single π, d, and π* orbitals and the respective MLCT and LC transitions. It is assumed that the d*-orbital lies at a significantly higher energy and that it does not lead to low-lying energy states. (b) From the two MLCT and LC transitions eight energy states are obtained: two singlets ^{1}**LC** and ^{1}**MLCT**, three ^{3}**LC**, and three ^{3}**MLCT** substates. The states can experience substantial quantum mechanical mixings due to configuration interaction (CI) and spin–orbit coupling (SOC). SOC induces the zero-field splitting (ZFS). After these quantum mechanical mixings, the terms singlet, triplet, LC, MLCT can no longer be regarded as "pure" classifications. For details, see Section 1.3.3.3. Here, we illustrate a situation in which the order of the d- and π-orbital does not necessarily lead to the same sequence of the corresponding triplets. It is remarked that the SOC path is only symbolized in (b), realistic requirements are discussed later (compare Fig. 1.9).

three-orbital model is characterized by just two excitations: one MLCT and one LC transition between the corresponding MOs (Fig. 1.6a).

In Section 1.3.1, it has been shown that each of these excitations results in one singlet and one triplet state. The electronic ground state is a singlet (Fig. 1.6b). Furthermore, according to the distinct spatial differences of the respective electron distributions in the involved orbitals, the exchange interactions – and thus the singlet–triplet splittings – differ strongly [see Eq. (3)]. For the π- and π*-orbitals of the ligands which are in the focus of this chapter, $\Delta E(^1\pi\pi^* - {}^3\pi\pi^*)$ is of the order of $10^4\,cm^{-1}$ (1.24 eV). On the other hand, $\Delta E(^1MLCT - {}^3MLCT)$ is much smaller, as the electron–electron interaction of the two electrons being distributed over the d-orbital and the spatially separated π*-orbital, respectively, is weaker. According to Ref. [70], $\Delta E(^1MLCT - {}^3MLCT)$ is about $3000\,cm^{-1}$ (0.37 eV), or even smaller. With this information, an energy level diagram is obtained as depicted in Fig. 1.6b.

Although the model for organo-transition metal compounds as presented in Fig. 1.6 is greatly simplified, it may still be used for an orientation and some general conclusions or helpful rules of thumb:

- In general, a HOMO/LUMO model does not contain singlet or triplet states.
- The relative positions of HOMO-1 and HOMO do not allow to predict the energy sequence of the corresponding triplet states directly. Figure 1.6 shows that **^{3}LC** can be the lowest state, although the HOMO–HOMO-1 sequence may suggest that **^{3}MLCT** might be the lowest state. This behavior is related to the difference in energy between HOMO and HOMO-1, which may be small in comparison to the energy difference between the exchange integrals.
- The number of states is quite large, even for this simple model. Eight states are obtained, two singlets (**^{1}LC**, **^{1}MLCT**) and $2 \times 3 = 6$ triplet substates (**^{3}LC**, **^{3}MLCT**) (neglecting double excitations, for example, to $d^2(\pi^*)^2$ configurations).
- The eight states can mix quantum mechanically induced by electron–electron interaction between the different configurations (configuration interaction, CI) and by SOC.[13] Especially, SOC between **^{1}MLCT** and **^{3}MLCT** and CI between **^{3}MLCT** and **^{3}LC** will alter the properties of the lowest triplet state (see Section 1.3.3.3). A splitting of the zero-order **^{3}LC** state into substates (ZFS) will result, the transitions between these and the ground state will become more allowed, the emission decay time will decrease, the photoluminescence quantum yield is mostly increased, and the spectra change, etc. (see Section 1.4.2. and Refs. [5, 70, 73, 74]).

1.3.3.2 Extended MO Model and Energy States

The simple model as discussed in Section 1.3.3.1 will certainly not be applicable for describing experimental results with sufficient quantitative precision. In particular, the number of electronic states is far from being realistic. This message is illustrated in Fig. 1.7 on the basis of two approaches, applied to discuss the example of $Ir(ppy)_3$. In a first introductory step, the discussion is restricted only to MLCT transitions; this approach is displayed in the inner frame of Fig. 1.7. Some group theory will help to find the number of d- and π^*-orbitals and, subsequently, the number of resulting energy states. In the electronic ground state, $Ir(ppy)_3$ has C_3 point group symmetry [113] and probably also in the lowest triplet state [114, 115].[14] In C_3 symmetry, the 5d-orbitals of t_{2g} representation split into

13) SOC is particularly important for third row transition metal complexes with open 5d shells. It increases approximately with Z^4, Z being the atomic number.

14) In Refs. [70, 73, 74, 114] it has been shown by low-temperature investigations that in homoleptic organo-transition metal compounds the lowest triplet state is delocalized over the three ligands and the metal. However, this result is only valid for a sufficiently large metal-induced ligand–ligand coupling. This coupling increases with a growing MLCT character of the lowest triplet state. A measure for this property represents the amount of ZFS (see also Sections 1.3.3.3 and 1.4). For example,